Available online at www.sciencedirect.com
ScienceDirect
Journal of Sound and Vibration 321 (2009) 454–470
JOURNAL OF SOUND AND VIBRATION
www.elsevier.com/locate/jsvi

Evaluation of lumbar vertebra injury risk to the seated human body when exposed to vertical vibration

H. Ayari[a], M. Thomas[a,*], S. Doré[a], O. Serrus[b]

[a]*École de Technologie Supérieure, Department of Mechanical Engineering, 1100 Notre-Dame Street West, Montreal, Quebec, Canada H3C 1K3*

[b]*École Nationale Supérieure de Mécanique et des Microtechniques, 26, Chemin de l'Épitaphe 25030 Besançon Cedex, France*

Received 11 January 2008; received in revised form 1 September 2008; accepted 19 September 2008
Handling Editor: S. Bolton
Available online 12 November 2008

Abstract

The objective of this research is to numerically determine the levels of vibration not to exceed accordingly to the corresponding dynamic stresses in the lumbar rachis when exposed to whole-body vibrations in order to identify the risk of adverse health effect to which professional heavy equipment drivers are particularly prone. A parametric finite element model of the lumbar rachis is generated in order to compute the modal parameters, the dynamic stresses and forces under harmonic excitations in a seated posture. The stress analysis reveals that the areas exposed to the highest fracture risk are the cancellous bone of the vertebral body as well as the vertebral endplate when vertical vibrations are transmitted from a seat to the lumbar spine of a driver. An injury risk factor has been developed in order to estimate the risk of adverse health effect arising from mechanical vibrations. It is shown that the injury risk factor increases with the age and consequently that the excitation amplitude must be limited to lower levels when age increases.

1. Introduction

Current literature reports evidence of the adverse health effects of whole-body vibration on the spinal system [1,2] and cites the many epidemiological studies conducted to establish a link between exposure to upper body vibration and low-back pain. Over the past 15 years, a number of published bibliographical reviews show higher occurrence of such disorders among populations exposed to dynamic loading, such as heavy equipment drivers, than among the general population [3]. However, the available epidemiological data are generally insufficient to establish a dose–effect relationship between exposure to whole-body vibration and the risk of lumbar disorders [4–7]. It is assumed that whole-body vibration induces dynamic stresses, mainly compressive, in the spine, producing microfractures in the endplates and vertebral body. The long-term exposure of the human body to vibration may lead to mechanical fatigue [8,9] and low-back problems due to microfractures in the bones (cortical and spongeous) and endplates, and to microlesions in the intervertebral

*Corresponding author. Tel.: +1 514 396 8603; fax: +1 514 396 8530.
E-mail addresses: Marc.thomas@etsmtl.ca, mthomas@mec.etsmtl.ca (M. Thomas).

0022-460X/$ - see front matter © 2008 Elsevier Ltd. All rights reserved.
doi:10.1016/j.jsv.2008.09.046

discs [10]. Various experimental studies aimed at evaluating fatigue behaviour in the human body under cyclic loading have shown that mechanical compressive dynamic stresses, principally in the lumbar spine, are sufficient to cause microfractures in the cancellous bone, which could lead to lower back pain [11–14]. Microfractures of individual trabeculae are commonly seen in human vertebrae [15]. Intracancellous microdamage also exist in vivo [16]. The fracture mechanism appears to be classic: microfractures observed in the vertebrae contribute to a reduction in vertebral rupture resistance [17]. The damage mechanism caused by fatigue in the cortical and cancellous bone can initiate and propagate cracks. Many in vivo experimental studies were undertaken to investigate human body response when exposed to mechanical vibration, including quantification of the resonant frequencies, vibration transmissibility, impedance, electromyography activity, spinal creep, and prediction of local forces and moments acting on the human spine. The in vivo natural frequency of the whole spine was measured in the 4–8 Hz range in the vertical direction for both standing and seated postures [18–22]. Subjective experiments have revealed humans to be more sensitive to vibration in this frequency range, based on comfort, fatigue and safety criteria [23]. To quantify the role of upper body vibration in structural changes and fatigue fractures to the spine entails an evaluation of the strains and stresses placed on spinal components. However, this is difficult or even impractical through experimental protocols or lumped parameter models. The finite element method may thus provide a better means for investigating stress analysis, by integration all of the anisotropic, inhomogeneous, and complex geometry of vertebrae. Several finite element models proposed in the literature examine the dynamic behaviour of the rachis and the entire spine. Kasra et al. [24] experimentally and numerically identify a natural frequency of 26 Hz based on one lumbar spine segment study, while Goel et al. [25] report, through their finite element model, a resonant frequency of 17.8 Hz, based on two lumbar spine segment studies (L4–S1). Izambert et al. [26] identified an anterior–posterior (AP) resonant frequency of 8.3 Hz based on in vitro testing of various motion segments of the lumbar spine and an average damping rate of nearly 10 percent. Kong and Goel [27] propose a finite element model of the upper body from the head to the sacrum (H-S1), consisting of a detailed representation of the lombosacral spine and a rough beam-type model of the thorax and cervical spine. Their results indicate a natural frequency of the global model (H-S1) at 8.32 Hz with the inclusion of the trunk muscles that reduces to 6.82 Hz when considering a preload of self-weight. These models are aimed at global predictions of the impedance and transmissibility due to dynamic loads transmitted from a vibrating seat to the human body [2]. Furthermore, numerical and experimental (in vitro or in vivo) tests have been carried out to predict the local forces and moments acting on the human spine. Kitazaki and Griffin [28] developed a 2D finite element model of the human body in order to study whole-body vibration. Beams, springs and mass elements were used in modelling the spine, viscera, head, pelvis and buttock tissue in the midsagittal plane. The model was validated by comparing the vibration mode shapes of the model with those measured in the laboratory. Buck and Woelfel [29] developed a dynamic 3D finite element model with a detailed representation of the lumbar spine and back muscles, comprising nonlinear ligament models, a nonlinear contact model in the articular facets, and dynamic properties of the passive and of active muscle tissue. The complete model of a sitting human was built by adding relatively simple dynamic models of the upper trunk with arms, a neck, a head, a pelvis and legs, using rigid bodies. Fritz [30] presents a human model—also made up of rigid bodies—for predicting the forces in the lumbar spine and neck. Pankoke et al. [31] presented a simplified, linearized version of the model developed by Buck and Woelfel [29]. Verver et al. [32] present a multibody human model consisting of a set of rigid bodies connected by kinematic joints, with the outer surface presented as a triangulated surface. In this model, all spinal and cervical vertebrae are represented by rigid bodies interconnected by 3D spring-damper combinations enabling a detailed analysis of the local loading occurring in the spine. The model allows the compression, tension and shearing forces to be predicted at different levels along the entire spine. These studies [28–32] provide useful information concerning the dynamic behaviour of the lumbar segments. They were aimed at computing the forces acting on the rachis without considering stress/strain distribution in the lumbar vertebrae for predicting the most critical zones at risk. Few numerical studies have established a relationship between dynamic stresses and seat acceleration [33]. By applying an analytical method, Thomas et al. [9] studied the long-term adverse health effects for drivers exposed to harmonic and random vibrations. However a more sophisticated numerical model is required to refine these results. On the other hand, the experimental study developed by Seidel et al. [13] allowed the relationship between the forces and seat acceleration to be assessed by considering posture, body type and body mass.

Furthermore, most of these numerical models use fixed parameters and are not designed to easily observe the effect of interindividual variations (posture, body type and body mass). It would appear that a finite element parametric model [34] is more suited to studying the various effects concerning anatomy or posture.

In the research described in this paper the aims were to study the dynamic behaviour and estimate the stress distribution in the lumbar vertebrae when exposed to low-amplitude mechanical vibrations, and, in so doing, help validate the assumption that whole-body vibration can induce microfractures in the bony elements of the spine, which, in turn, can lead to adverse health effects [11–14]. The investigated populations are professional drivers. The study has two specific objectives. Firstly, it is aimed at validating the dynamic behaviour of a parametric finite element model whose geometry is based on the parametric model proposed by Lavaste et al. [34] and that was applied to static analysis. Validation is conducted by comparing natural frequencies and vibration transmissibility to the related numerical and experimental results in the literature. Secondly, a new predictive relationship between the mechanical stresses in the vertebrae and seat acceleration is established in order to estimate the risk of damage. Stress distribution in the vertebrae of the lumbar rachis is computed for an average body type driver in a seated position and exposed to vertical vibration. Driver age and the corresponding osseous density are considered in order to determine the limits of seat acceleration.

2. Methods

2.1. Finite element models

Three models have been developed: one considers a single motion segment (L4/L5); one considers the lumbar region of the spine (L1/L5), composed of four motion segments; and one considers the thoracic and lumbar regions of the spine (T1/L5), composed of 16 motion segments. A finite element model of the lumbar spine (L1–L5) was generated in using CAD software. The parametric equations describing the shape of a vertebra and an intervertebral disc as established by Lavaste et al. [34] were considered, and the morphometric dimensions as measured on various vertebral bodies by Berry et al. [35] were applied. Fig. 1 illustrates the main parameters of lumbar vertebrae.

The main advantage of using a parametric model is the facility with which different human morphologies can be studied. A parametric dynamic model presents the advantage of simulating any condition of seated posture as well as the effect of interindividual geometrical variations. The parametric model allows for studying the effect of the sitting posture, bone structure and body mass on the mechanical behaviour of a spine exposed to whole-body vibration. The present study shows the results for an intermediary body type corresponding to an average size weighing 75 kg and seated in a normal posture (lumbar curve of $\theta = 15^{\circ}$). The sensitivity of parameters being the object of other studies, the morphologic parameter has not been changed in this paper. However, the density and damping rate were varied. Fig. 2 illustrates curves of the lumbar spine.

Each model of the lumbar spine is composed of 33 bodies (annulus, nucleus, endplate, cortical shell and spongy bone); 54 contact zones are defined between the bodies. The volumes of each part of the model were meshed separately with their meshing parameters. Owing to the geometrical complexity of the spine, the finite element mesh had to be fairly fine. The cortical shell, posterior elements, cancellous bone and endplates were meshed using 3D 10-node tetrahedral elements (Ansys software: Solid 187). This type of element was selected because it facilitates the interpolation of external geometry. The nonhomogeneous structure of the intervertebral disc was taken into account; as is done in other finite element models [24,25], the annulus

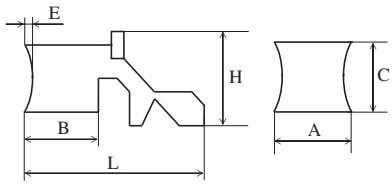

Fig. 1. The main parameters of lumbar vertebrae [34].

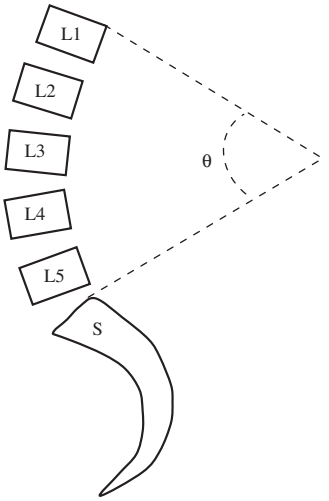

Fig. 2. Curves of the lumbar spine. The angle θ illustrates the lumbar curve in sitting position: lordosis posture, $\theta \geqslant 25^{\circ}$; flexed posture, $\theta \leqslant 5^{\circ}$; and intermediate posture, $\theta \approx 15^{\circ}$.

fibrosus was modelled as composite material. The behaviour of the nucleus pulposus was modelled using volumic elements with a Poisson coefficient of 0.499 representing a quasi—isovolumic behaviour. The contacts were modelled with contact elements (Target 170 with 8-node, and Conta 174 with 8-node). In vivo, relative motion between posterior elements was assured by articular cartilage. In the model, a very low friction coefficient was applied to model the relative motion of cartilaginous structures. A frictionless contact element was chosen to model the connection between the posterior elements. Low-rigidity springs were added to the contact element model to ensure continuity. While the thickness varies from minimal in the central region to maximum at the ends, the endplate was modelled by considering a very thin layer (0.5 mm thick). Thus it inherently provides little additional strength. Furthermore, it may serve to distribute the load more evenly over the vertebral bone, while preventing the migration of softer nucleus material into the pores in the vertebral endplate. The aspect of bone remodelling, while very important in fatigue concept, has not been considered in this study which is aimed at developing a criteria based on an instantaneous injury risk of fracture (IRF). The IRF contains the information on ultimate stress and consequently on ageing by varying density and damping. The total number of lumbar spine elements and nodes is approximately 36,500 and 83,808, respectively. The meshing of the lumbar spine and frictionless contact between apophyses is shown in Fig. 3.

Once the rachis model has been generated, dynamic analyses may be carried out on the numerical model. In order to validate our parametric finite element model and conduct a harmonic analysis, modal and harmonic analysis were performed on one motion segment (L4/L5), on the rachis (L1/L5), and on the partial spine (T1/L5). Lastly, the dynamic stress/strain distribution on the rachis was computed. To compute the natural frequency of the entire spine, an approximated model of the partial spine (T1–L5) was generated. The thoracic (T1–T12) structure was generated using the parametric model of L1. Curve angles were introduced for a sitting posture based on the values of the lumbar lordosis (angle $\theta = 15^{\circ}$: average posture) and of the dorsal kyphosis [36]. Different equivalent masses representing the upper part of the body were applied to each model. The mechanical properties of the various elements (cortical shell, cancellous bone, posterior elements and cartilaginous endplates) forming the vertebral body were deduced from the literature [24,25,27,34,37,38]. The static properties are provided in Table 1.

For the modal analysis of the lumbar rachis, the displacements of the lower face were blocked in all directions. A distributed mass of 40 kg modelling the upper body was applied to the upper face of the rachis: $\approx$57 percent of the body weight [9,24]. The lower face of L5 was fixed. Within the framework of harmonic analysis, the lower face was subjected to various vertical accelerations ranging from 0.63 to 4 m s^{-2}. These acceleration amplitudes were chosen in the range that can be met in industry in order to represent a range from very low risk to high risk. These values are in accordance with the values defined in ISO 2631-1 [23] curves for

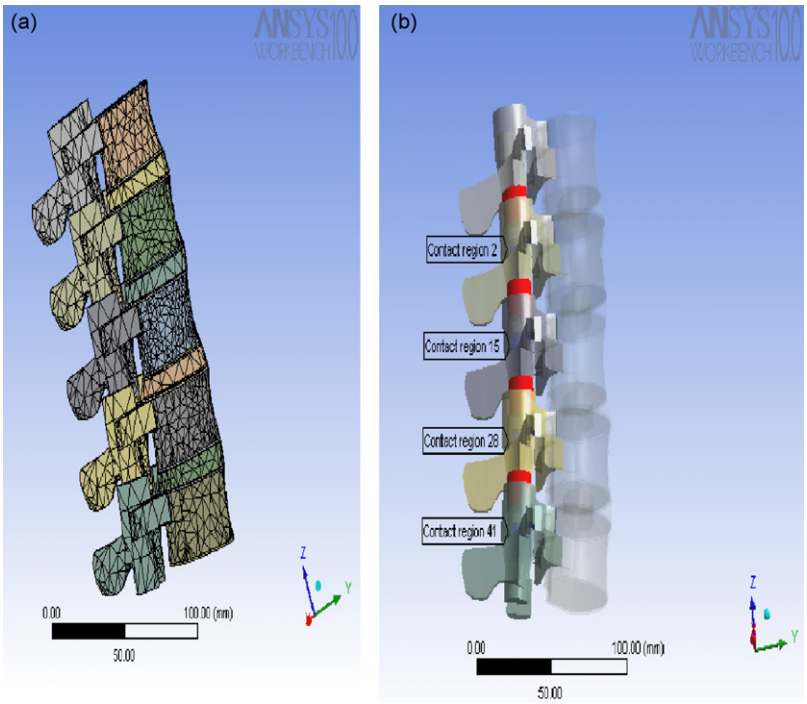

Fig. 3. Finite element models: (a) lumbar spine and (b) contact between posterior elements.

Table 1
Material properties

Material	Element type	Elastic modulus (MPa)	Poisson's ratio
Cortical bone	Volumic	12000	0.3
Posterior elements	Volumic	1000	0.25
Cancellous bone	Volumic	100	0.2
Cartilaginous endplate	Volumic	24	0.4
Annulus fibres	Volumic	500	0.3
Annulus matrix		4.2	0.45
Nucleus	Volumic	1.3	0.499

describing the vertical acceleration exposure limits based on frequency and duration. In order to simulate the effects of mechanical shock [39] encountered on rough roads, the vibration response at resonance was also analysed by inputting very high levels of seat acceleration (10, 20 and 40 $m\,s^{-2}$). The viscous damping rate depends on the degree of intervertebral disc degeneration (disc grade) and muscle activity [27]. Since the damping rate can vary between humans, transmissibility analysis was carried out using different viscous damping rates (0.08, 0.1, 0.2 and 0.3). The stress response curves were evaluated by considering a viscous damping rate of 0.1 as determined from the experiments of Kasra et al. [24] and Izambert et al. [26].

3. Results

3.1. Modal analysis

Table 2 reports the first four natural frequency values representing the AP mode, lateral mode, axial mode and torsional mode for the three models.

Table 2
Natural frequencies for different numbers of motion segments

Mode no.	Type of mode	Segment L4/L5 $M_{eq} = 40$ kg (Hz)	Lumbar spine L1/L5 $M_{eq} = 40$ kg (Hz)	Partial spine T1/L5 $M_{eq} = 40$ kg (Hz)
1	AP	6.5	1.4	0.28
2	Lateral	7.7	1.7	0.32
3	Axial	27	13.9	4.7
4	Torsional	158	74.7	12.44

The AP resonant frequency computed for a single motion segment (L4–L5) is around 6.5 Hz, while the axial frequency is about 27 Hz. The axial and AP frequencies correspond closely to the numerical tests presented by Kasra et al. [24] and Guo and Teo [40], carrying a distributed mass of 40 kg. Based on the data from a parameterized geometrical model and on the morphometric data of the existing lumbar rachis (L1–L5) [34,35], the natural frequencies of the AP and axial modes are around 1.41 and 13.88 Hz, respectively. The first four mode shapes of the rachis, associated with their natural frequencies, are presented in Fig. 4.

These frequencies correspond closely to the numerical results obtained by Kong et al. [27] (2 Hz for the AP mode and 10.6 Hz for the axial mode) on a finite element model (L1–S1), as well as with those obtained by Guo and Teo [40] on finite element model (L1–L5) carrying a distributed mass of 40 kg (11.5 Hz for the axial mode). A modal analysis was carried out on the partial spine (T1–L5). By generating a model of the partial spine, which respects the curvatures and connections between the articular facets of the vertebrae, the natural frequencies of the AP and axial modes (around 0.28 and 4.7 Hz, respectively) (Fig. 4) correspond to findings in the literature [9,19,21,22]. These values also compare well with in vivo measurements and subjective perceptions, which revealed a natural frequency of the vertical column between 4 and 8 Hz [18,20,23]. As expected, the modal analysis shows the natural frequencies in the AP and axial directions to decrease with a greater number of motion segments, and to increase when fewer motion segments are considered. For example, the vertical resonant frequency for one motion segment (e.g.: L4–L5) is approximately 27 Hz, whereas it is around 13.88 Hz for the rachis and decreases to 4.7 Hz for the whole spine. The good correlation between the modal analysis results obtained from the parametric model and those obtained from experimental tests indicate that the developed model is representative of the reality.

3.2. Vibration transmissibility of the rachis

Vibration transmissibility (L_i/L5) is the ratio between the computed dynamic response with respect to the L_i vertebral body ($i = 1,\ldots,5$) and the dynamic input applied at the seat (L5). The vibration transmissibility varies according to the viscous damping rate. The transmissibility computed from L5 to L1 (L1/L5) was studied for various damping ratios ranging from 0.08 to 0.3 (Fig. 5).

The maximum transmissibility ratio (L1/L5) computed from the rachis model reaches 5.4 for a damping ratio of 8 percent and 1.7 for a damping ratio of 30 percent. The transmissibility values predicted by this study are also very close to the results obtained by Kong et al. [27] and Verver et al. [32]. For a damping ratio of 30 percent, Kong et al. [27] found a maximum transmissibility of 1.3 at L1. Verver et al. [32], through their in vivo measurements, determined a maximum transmissibility of around 2 at T1, while Dupuis [18,20], through experiments, yielded the same result at L3–L4. Indeed, Izambert et al. [26] measured a maximum transmissibility of 5 on various in vitro motion segments, whereas our model yields a transmissibility of about 4.4 for a damping coefficient of around 10 percent. The computed results thus appear very acceptable for damping ratios ranging from 8 to 30 percent. We noted that the transmissibility decreases from a vertebral level L_i to a vertebral level L_{i+1}. Fig. 6 shows the various transmissibility ratios computed for L1/L5, L2/L5 and L3/L5 for an excitation applied at L5 by considering a viscous damping rate of 0.3 for an average body type.

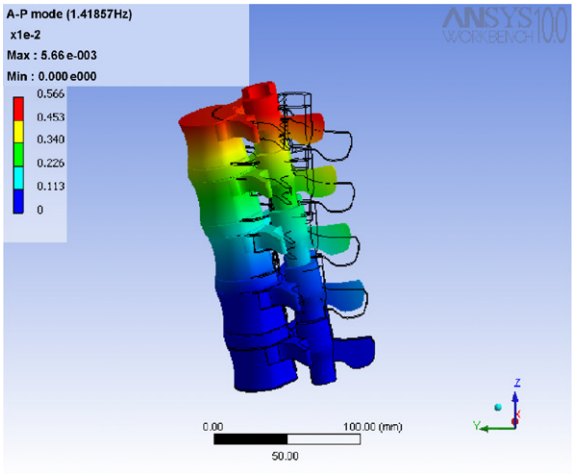

AP mode, f=1.41Hz

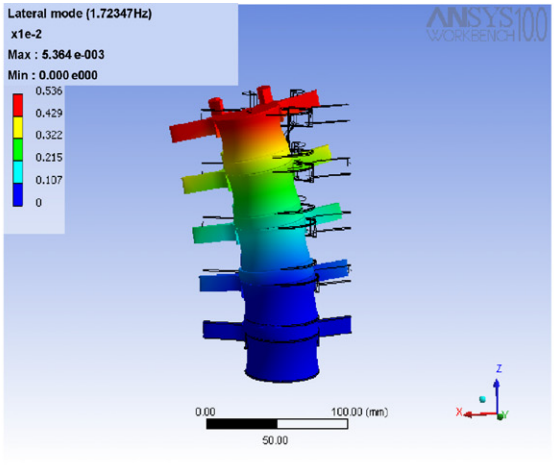

Lateral mode, f = 1.72 Hz

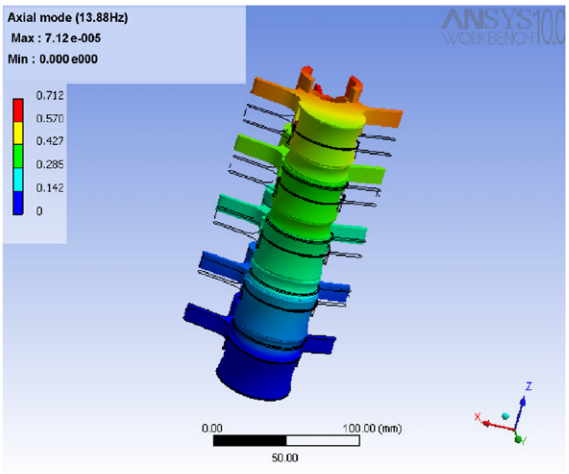

Axial mode, f = 13.88 Hz

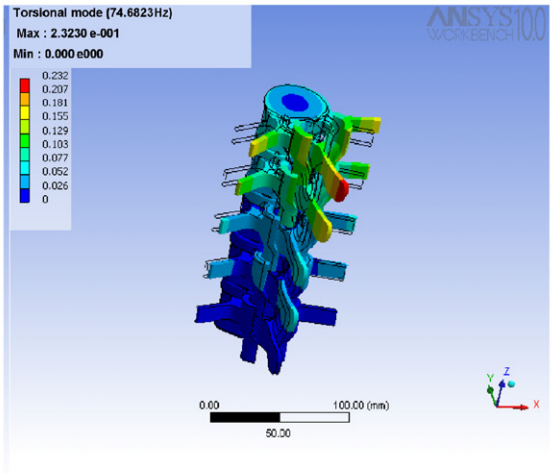

Torsional mode, f = 74.68 Hz

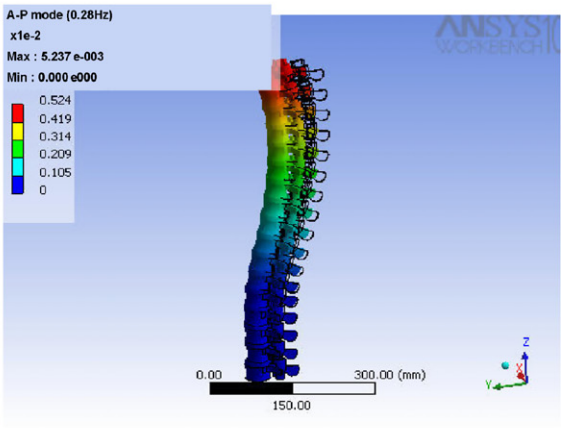

AP mode, f=0.28Hz

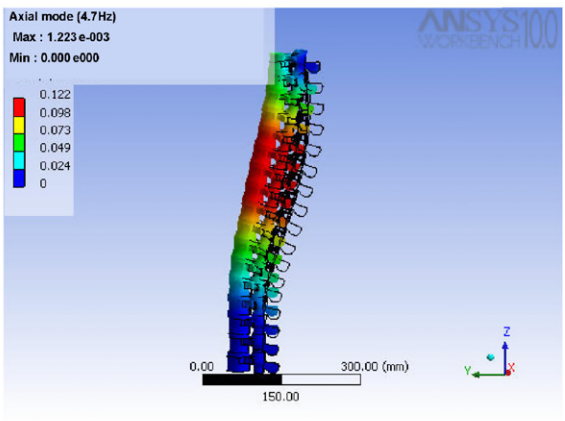

Axial mode, f = 4.70 Hz

Fig. 4. Mode shapes of lumbar spine (L1/L5) and partial spine (T12/L5).

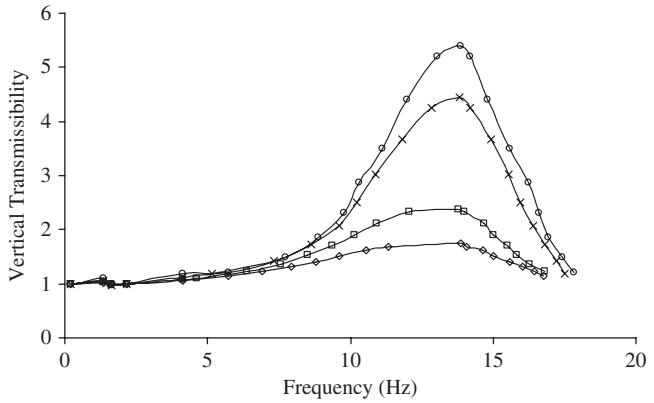

Fig. 5. Effect of damping ratio on transmissibility ratio at the L1–L5 vertebrae: —○— $\zeta = 0.08$, —×— $\zeta = 0.1$, —□— $\zeta = 0.2$, and —◇— $\zeta = 0.3$.

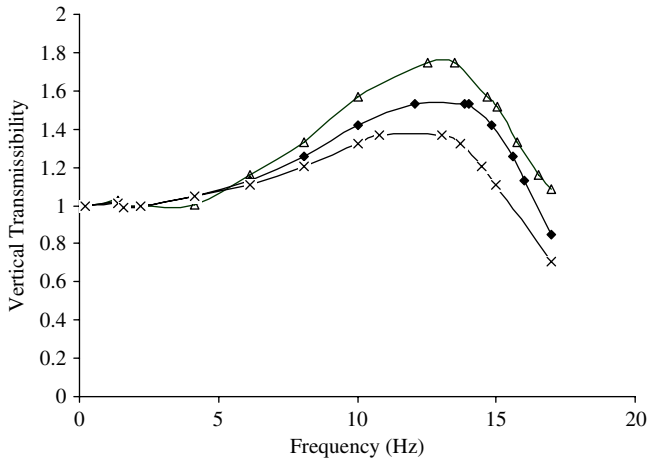

Fig. 6. Transmissibility at different vertebral bodies according to vertical vibration imposed at the bottom of L5 ($\zeta = 0.3$): —△— L1, —◆— L2, and —×— L3.

The amplitude at 1.41 Hz, which corresponds to the AP mode of the lumbar spine, is small, while the graph properly highlights the magnitude of vertical vibration transmitted from seat to human body, with a peak at 13.88 Hz. These computed results correlate well with the published data [2,23] and help validate the model.

3.3. Dynamic stress analysis of the spine

The dynamic stresses have been computed in various components of the lumbar rachis for different acceleration levels, taking into consideration a viscous damping rate of 10 percent. This stress study identifies the vertebrae most susceptible to damage when exposed to whole-body vibration and thus helps identify the critical components. The stresses were obtained by vertically applying an acceleration level of 3.15 m s^{-2} to the seat at the natural frequency of 13.88 Hz. This level of acceleration was chosen in order to compare the results with those from literature. The excitation frequency was chosen at the natural frequency of rachis in order to obtain the same behaviour as can be met in random or transient vibrations. As expected, the numerical results reveal that the compressive stresses applied to the rachis decrease when moving away from the fixed base. Stress values close to the boundary conditions have been neglected because the stress concentration

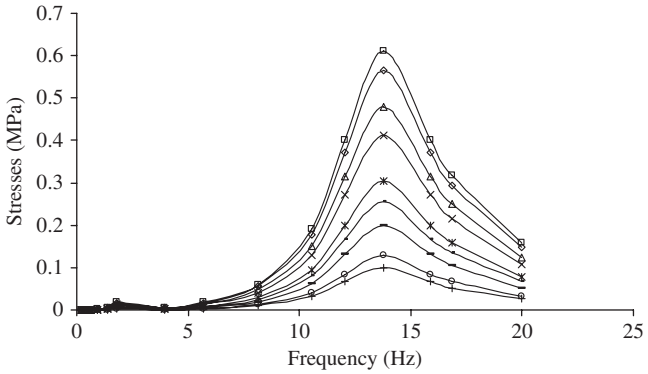

Fig. 7. Stresses at the L5 cancellous bone with frequency for different acceleration amplitudes: $a = 4\,\mathrm{m\,s^{-2}}$, $a = 3.7\,\mathrm{m\,s^{-2}}$, $a = 3.15\,\mathrm{m\,s^{-2}}$, $a = 2.7\,\mathrm{m\,s^{-2}}$, $a = 2\,\mathrm{m\,s^{-2}}$, $a = 1.6\,\mathrm{m\,s^{-2}}$, $a = 1.25\,\mathrm{m\,s^{-2}}$, $a = 0.8\,\mathrm{m\,s^{-2}}$, and $a = 0.63\,\mathrm{m\,s^{-2}}$.

was too localized and showed overestimated values. For an average body type seated in a normal posture (lumbar curve of $\theta = 15^{\circ}$), the stresses applied at L5 reach 0.48 MPa in the cancellous bone of the vertebral body, 6 MPa in the cortical shell, and an average of 0.42 MPa in the endplate of the L4–L5 interface. It is noted that the distribution of compressive stresses in the cancellous bone appears homogeneous on all vertebrae (even for the endplate), whereas the state of stress increases from L1 (4 MPa) to L5, and reaches 6 MPa at the level of the cortical shell of L5. The vertebral cortical shell shows a higher stress level than the central core of cancellous bone. However, this does not indicate a higher risk of fracture in the cortical shell, since the ultimate stress of cortical bone is about 50 times greater than that of cancellous bone. AP stress distribution also increased from L1 to L5 and shows stresses of up to 0.16 MPa at the level L3–L4 interface, and of up to 0.2 MPa at the level L4–L5 interface when applying an acceleration level of $3.15\,\mathrm{m\,s^{-2}}$ to the vertical resonance (13.88 Hz). The stress response in the L5 cancellous bone was also computed for different seat acceleration amplitudes. Fig. 7 shows the stress response on the cancellous bone of vertebra L5 for various accelerations ranging from 0.63 to $4\,\mathrm{m\,s^{-2}}$.

Fig. 7 shows that the stress can reach a value of 0.62 MPa when applying an acceleration of $4\,\mathrm{m\,s^{-2}}$ and 0.48 MPa for an acceleration of $3.15\,\mathrm{m\,s^{-2}}$ applied at its vertical natural frequency. When applying very high acceleration amplitudes such as 10, 20 and $40\,\mathrm{m\,s^{-2}}$ to investigate shock response, it was observed that the stresses can reach severe stress levels of 1.6, 3 and 6.3 MPa, respectively, in the L5 cancellous bone.

3.4. Force analysis of the spine

Compressive and tangential forces have been computed at the L3–L4 motion segment level, chosen to allow us to compare our results with those found in the literature. For an acceleration of $3.15\,\mathrm{m\,s^{-2}}$, the maximum stresses observed for an average body type on the cortical bone (L5), posterior arch, cancellous bone and cartilaginous endplates are, respectively, about 6, 0.8 and 0.48 MPa, with an average of 0.42 MPa when excited at a natural frequency of 13.9 Hz. While the static force is computed at 400 N for an average body type, the dynamic maximum compressive force computed at L3–L4 with a damping rate of 10 percent is computed at 630 N at the vertical resonance frequency by applying acceleration amplitude of $3.15\,\mathrm{m\,s^{-2}}$. The dynamic compressive force was estimated using the average compressive stress on the L3–L4 endplate level ($\sigma_c = 0.42$ MPa), multiplied by the area of the endplate ($S = 1500\,\mathrm{mm^2}$). The maximal compressive force, combining static and dynamic efforts ($\mathrm{Fc_{stat}} + \mathrm{Fc_{dyn}}$) and acting at L3–L4 segment is 1030 N. The maximum AP force was evaluated at 240 N (shear stress multiplied by endplate surface S). These forces can be estimated for various acceleration amplitudes applied to the seat. In the literature, few articles appear to deal with the dynamic forces applied to the lumbar spine. Through experiment, Fritz [30] determined a maximum load at level L3–L4 of 634 N for an acceleration of about $4.9\,\mathrm{m\,s^{-2}}$. Verver et al. [32] estimated the compressive and

Table 3
The L3–L4 maximum compressive forces compared to those published in literature

	Frequency range (Hz)	Max. acc. (m/s^2)	Compression (N)
Present study	0.5–15	3.1	1030
Thomas et al. [9]	4–6	3.1	980
Verver et al. [32]	0.5–15	4	581–852
Fritz [30]	0–30	1–5	634
Hinz et al. [41]	0.5–7	3.1	657

tangential loads on the whole spine (from interface L5–S1 to interface C1–C2). At resonance, the compressive load on level L3–L4, for an acceleration of $3.9\,m\,s^{-2}$, ranged from 581 to 852 N according to type of seat. Hinz et al. [41] developed a biomechanical model for determining the compressive load at level L3–L4 by using an effective human body mass on L3–L4 and a relative acceleration of $2.9\,m\,s^{-2}$. The maximum load was estimated at 657 N (Table 3). Through an analytical model, Thomas et al. [9] estimate a compressive force about 980 N for seat acceleration greater than $3.15\,m\,s^{-2}$. Table 3 shows that the forces revealed by this study are higher than those in related literature; this is due to the fact that the excitation was applied at the natural frequency of the system.

4. Injury risk factor

A new damage index has been developed for predicting the risk of exceeding a certain percentage of the material's ultimate stress capacity and consequently developing microfractures. This damage index is called the IRF. The IRF has been defined as the ratio between the computed total stress ($\sigma_{dyn}+\sigma_{stat}$) and the ultimate stress (σ_u) for each type of bone:

$$\mathrm{IRF}(\%) = 100\,\frac{\sigma_{stat}+\sigma_{dyn}}{\sigma_u}. \tag{1}$$

The ultimate stresses or forces were extracted from the literature for healthy persons. Table 4 presents the IRF computed at the various components of vertebra L5, exposed to a $3.15\,m\,s^{-2}$ acceleration amplitude in vertical acceleration at its natural frequency, by considering an average body type with a damping rate of 10 percent.

Similarly, the IRF was computed in the L5 cancellous bone according to the vibration frequency ranging from 0 to 15 Hz, for various acceleration amplitudes (Fig. 8). The IRF was computed by applying acceleration amplitudes ranging from 0.63 to $4\,m\,s^{-2}$ to the seat, in order to consider dynamic excitation consisting of low-amplitude vibration, as is normally encountered in vehicle vibration [7].

The stress analysis shows that the risk of damage is highest for the cartilaginous endplate (24 percent) and cancellous bone (25 percent). These observations are perfectly coherent with the results of the experimental fatigue tests on vertebral motion segments exposed to mechanical vibration carried out by Hansson et al. [11] and Ruth et al. [42]. During their static and dynamic compression tests (high amplitude vertical vibration), these authors observed that the most critical elements as regards fractures were the cartilaginous endplate and the cancellous bone. We note that for accelerations close to $3.15\,m\,s^{-2}$, the instantaneous risk of fracture remains weak for a young and healthy driver. However, in the long term, it can lead to bone microfractures through mechanical fatigue, especially when the IRF factor is greater than 30 percent, as it is usual in fatigue problems. Thus, we assume an IRF of about 30 percent as the limit of endurance for avoiding fatigue problems. In addition, this study demonstrates that, if acceleration exceeds $10\,m\,s^{-2}$, as it can be encountered on very rough roads (shocks), the IRF exceeds 50 percent. A similar result was predicted by Morrison et al. [39], who employed a health hazard method. These authors found a probability of injury of close to 95 percent for drivers exposed to repetitive shocks of 2 g at 6 Hz (close to the spine natural frequency) during a one-year exposure.

Table 4
Injury risk factor computed for an average body type

	σ_u (or force)	σ_{dyn} (or force) (for $A = 3.15\,m/s^2$)	σ_{stat} (or force)	IFR = 100 $(\sigma_{dyn}+\sigma_{stat})/\sigma_u$ (percent)
Cortical shell	160 MPa [48]	6 MPa	3.36 MPa	5.8
Cancellous bone	3 MPa [43,44]	0.48 MPa	0.26	25
End-plate	3.3 MPa [42]	0.42	0.38	24
Whole vertebrae	5400 N [11,12]	630 N	400 N	19

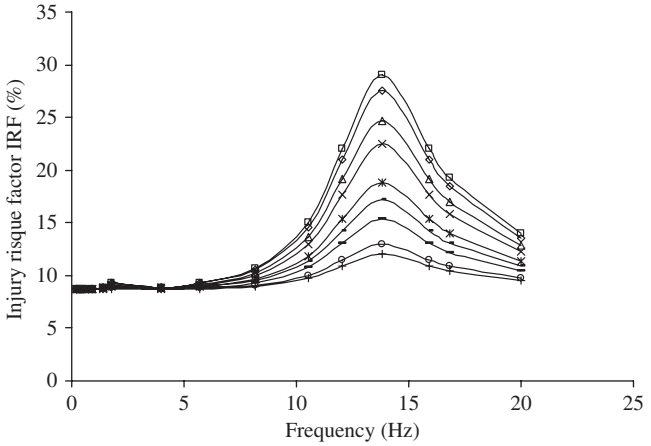

Fig. 8. Injury risk factor with frequency at the L5 cancellous bone for different acceleration amplitudes: $a = 4\,m\,s^{-2}$, $a = 3.7\,m\,s^{-2}$, $a = 3.15\,m\,s^{-2}$, $a = 2.7\,m\,s^{-2}$, $a = 2\,m\,s^{-2}$, $a = 1.6\,m\,s^{-2}$, $a = 1.25\,m\,s^{-2}$, $a = 0.8\,m\,s^{-2}$, and $a = 0.63\,m\,s^{-2}$.

5. Discussion

Validation of the bony microfracture assumption as a source of adverse heath effects requires, as a first step, knowledge of stress/strain distribution in the lumbar spine in order to locate the vertebral elements most likely to be damaged. The consistencies between the developed model and the published results on loading forces and natural frequencies demonstrate that the computed stresses for the L5 cancellous bone are representative (Fig. 7) and constitute a significant contribution to the understanding of bone fractures. A relationship has been established between the resulting dynamic stresses and the input acceleration amplitudes as measured at the seat. By extracting information from Fig. 7, which related the dynamic stresses as a function of frequency for different acceleration amplitudes, a linear relationship has been developed between the dynamic stresses σ_{dyn} (MPa) and the acceleration amplitudes a ($m\,s^{-2}$) measured at the seat when excited to the rachis resonant frequency. By considering the static stress component (MPa), which has been computed at 0.26 MPa, the total stress σ_{tot} is equal to $\sigma_{tot} = \sigma_{dyn} + \sigma_{stat}$. A linear least-square regression revealed the following relationships between the total stress (static and dynamic) σ_{tot} computed from the maximal level and from a mean level with the acceleration A measured at the seat:

$$\text{Max stress}: \ \sigma_{tot} = 0.16A + 0.27, \tag{2}$$

$$\text{Mean stress}: \ \sigma_{tot} = 0.13A + 0.22. \tag{3}$$

To validate our numerical model, relations Eqs. (2) and (3) were compared with an experimental model established by Seidel et al. [13]. In fact, these authors [13] proposed an experimental model to estimate the mean dynamic and total stresses. The static stresses were found to be related to posture, age and body mass.

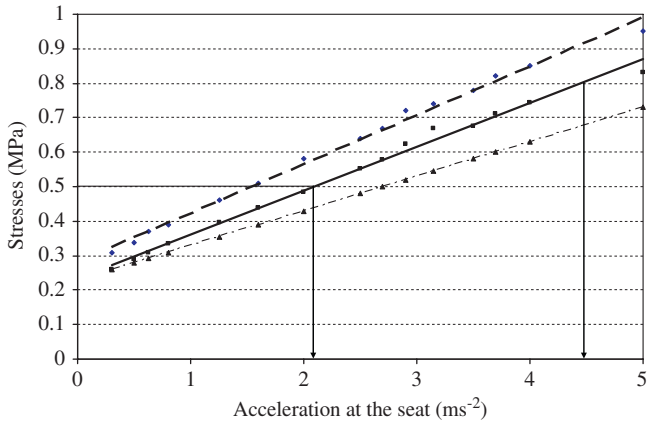

Fig. 9. Total stress with seat acceleration, at resonant frequency: ▬ ▬ ▬ max stress and ▬▬▬ mean stress obtained by our numerical model; and - · - · - Seidel experimental model.

The dynamic stresses were related to body type, posture and seat acceleration. Through in vivo tests applied to 36 subjects, they determined a linear relationship between the dynamic stresses (MPa) and the acceleration amplitudes ($m\,s^{-2}$). By considering a 40-year-old male in the driving posture, which, in our study, corresponds to an average body type, and by generating a static stress component of 0.21 MPa, a linear regression analysis, applied to L5/S1, revealed the following relationship:

$$\text{Mean stress}: \ \sigma_{\text{tot}} = 0.1A + 0.23. \tag{4}$$

Fig. 9 illustrates the relationships Eqs. (2)–(4) for an average body type, computed at the natural frequency of the lumbar spine in the vertical direction. It shows that the stresses obtained from our numerical results may be advantageously compared to the experimental model as proposed by Seidel et al, for the same anatomy.

To simplify the analysis, a discrete single degree of freedom model (1 dof) was adopted by Coermann [49] and Griffin [2] for modelling the human body exposed to mechanical vibrations. By applying an excitation to the natural frequency, the dynamic stress computed for a 1 dof system can be expressed in the following form:

$$\sigma_{\text{dyn}} = \frac{\sqrt{1+2(\xi)^2}}{2\xi}\frac{A*M}{S}\cos(\theta), \tag{5}$$

where M is the equivalent mass, A the applied acceleration amplitude to the seat, S the average cross-section of disc, θ the posture angle and ξ the damping rate.

The vibration transmitted to the seat during driving comes from road roughness that can generate multiple shocks and random vibration. These vibrations are transformed along its path by the natural frequencies of the suspension and the result is a superposition of harmonic motion with random vibration and shocks. In the case of random excitation, a different approach from harmonic excitation must be adopted for estimating the fatigue damage, because all the frequencies are excited in the same time and the natural frequency of the lumbar spine is always excited. Indeed, we may consider that this study represents a critical severity case. Then, our study furnishes a method for estimating the dynamic stresses and the IRF, considering ageing, in case of random excitation when the natural frequencies of the lumbar spine are all excited.

In this study, the static stress σ_{stat} is 0.26 MPa, the applied mass is approximately 57 percent of the body weight ($\approx$40 kg), the average disc cross-section at L3–L4 is 1500 mm^2, the rate damping is 10 percent and the posture angle is about 15°. The total stress σ_{tot} ($\sigma_{\text{dyn}}+\sigma_{\text{stat}}$) can then be expressed as following:

$$\sigma_{\text{tot}} = 0.14A + 0.26. \tag{6}$$

This simplified model corresponds closely to the models obtained from our numerical results (Eqs. (2) and (3) for mean and max stress, respectively).

Since the IRF (percent) was defined as the ratio between the computed total stress ($\sigma_{\text{dyn}}+\sigma_{\text{stat}}$) and the ultimate stress (σ_u), we can also determine a linear relationship between the IRF and the acceleration

amplitude applied at the seat. For example, if we consider the ultimate stress for a healthy trabercular bone (one of the osseous locations most susceptible to vibratory damage) as averaging $\sigma_u = 3$ MPa, the relationship relating the IRF (percent) to the acceleration amplitude a ($m\,s^{-2}$) becomes therefore:

$$\mathrm{IRF}\,(\%) = 5.3A + 9. \tag{7}$$

We can conclude that the stress limits issued from our study agree very well with those exposed in ISO 2631-5 [50] when drivers are subjected to vibrations containing multiple shocks. In fact, in many cases, such as in machinery travelling over rough surfaces, dynamic loading could be considered as vibration containing multiple shocks. A method for estimating vibration containing multiple shocks has been produced by ISO 2631-5 [50], which is concerned with the lumbar spine response. For impact excitation, the ISO 2631-5 [50] standard proposes a procedure for estimating the daily equivalent static compression dose σ (MPa). It computes the lumbar spine acceleration from the time histories in the seat, by using a theoretical model and extracted the peaks $A_i\,(i = 1 \ldots n)$ of the lumbar response in each direction. In lateral directions, the theoretical model is assumed to be linear and acceleration peaks are counted in negative and positive direction while in vertical direction, the theoretical model is extracted from a neural network model and the peak acceleration is only counted in positive direction. The corrected acceleration dose is computed in each direction and a daily equivalent static compression dose σ (MPa) is proposed as follows:

- if $\sigma < 0.5$ MPa, a 20 years old man working 240 days a year will have a low probability of injury;
- if $0.5 < \sigma < 0.8$ (MPa), a 20 years old man working 240 days a year will have a moderate probability of injury;
- if $\sigma > 0.8$ (MPa), a 20 years old man working 240 days a year will have a high probability of injury.

By considering an intermediate sized person, Fig. 9 shows that the stresses of 0.5 and 0.8 MPa are corresponding to acceleration levels of between 2.1 and 4.5 $m\,s^{-2}$, respectively. Consequently, it may be suggested from ISO 2631-2004 [50] that a healthy driver working 240 days a year will have a low probability of injury if acceleration amplitude is controlled lower than 2.1 m/s^2 at the seat and that a healthy driver working 240 days a year will have a high probability of injury if the vibration amplitude at the seat is higher than 4.5 m/s^2. This high level of acceleration of 4.5 m/s^2 is coherent with ISO 2631-1997 [23] which recommends an exposition time lower than 30 min a day in this case. Dealing with acceleration data measured at the seat presents the great advantage to be easier to manipulate for industry than dealing with spine stresses than cannot be measured in vivo.

The cancellous bone, representing almost 90 percent of the total volume of the vertebrae, has a porous structure and its fundamental role is to absorb energy. The cancellous bone has anisotropic mechanical properties that depend on the porosity of the specimen. The elastic and strength properties of cancellous bone are displaying substantial heterogeneity with respect to age, health, anatomy site, loading direction, and loading mode. In compression, both modulus and strength decrease with age, falling approximately 10 percent per decade [43]. Both modulus and strength depend heavily on apparent density. These relationships vary for different types of cancellous bone due to the anatomic site, age, disease and related variations in cancellous architecture. Linear and power-law relationships can be used to describe the dependence of modulus and compressive strength on apparent density and age [43–45], with typical coefficients of determination (R^2) ranging from 0.6 to 0.9. The apparent density of vertebral cancellous bone decreases linearly with ageing [46,47]. The age of the vertebral cancellous bone samples studied ranged from 20 to 80 years and the average density was $0.23 \pm 0.08\,g\,cm^{-3}$, varying from 0.05 to $0.3\,g\,cm^{-3}$ [46,47]. Thus, the IRF can be expressed according to the acceleration amplitude at the seat, age and corresponding osseous densities. Fig. 10 shows the relationship between the IRF and the acceleration amplitudes recorded at the seat when excited to the rachis natural frequency for different osseous densities and corresponding ages.

As expected, the results show that the risk of damage increases with age due to the corresponding decrease in osseous density. By considering a healthy person and by applying acceleration amplitude about 4.5 $m\,s^{-2}$ at the lumbar spine, an excitation at the natural frequency can produce a risk of damage of 30 percent for a 45-year-old driver by considering an apparent density of $0.23\,g\,cm^{-3}$. As described in Fig. 10 for a 65 years old man, an acceleration amplitude between 2.1 and 4.5 $m\,s^{-2}$ (producing a total stress between 0.5 and 0.8 MPa as

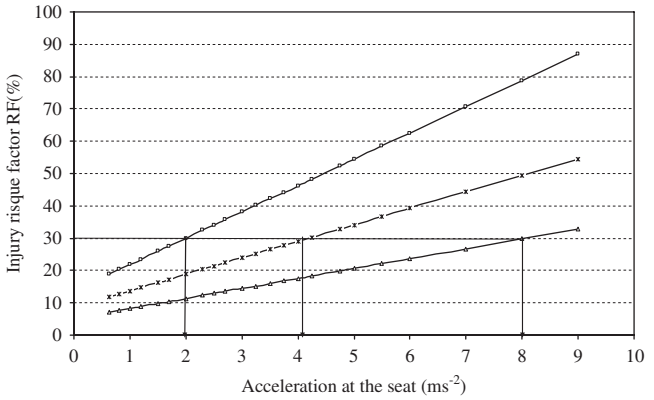

Fig. 10. Injury risk factor with acceleration amplitude at the seat, at resonant frequency for different ages and osseous densities: — □ —65 years; apparent density $\rho = 0.18\,\mathrm{g\,cm^{-3}}$, — × —45 years; apparent density $\rho = 0.23\,\mathrm{g\,cm^{-3}}$, and — △ —25 years; apparent density $\rho = 0.3\,\mathrm{g\,cm^{-3}}$.

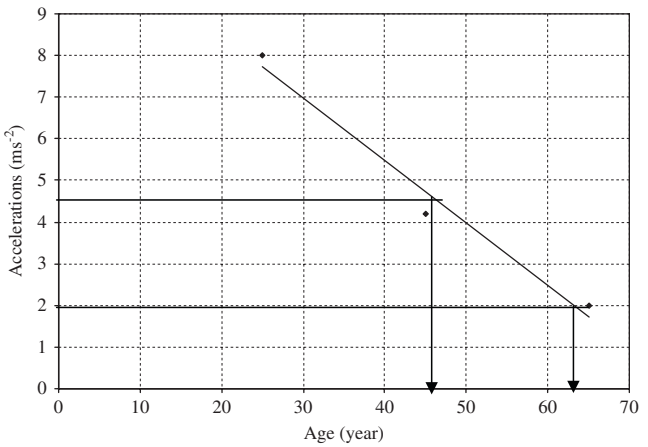

Fig. 11. Acceleration threshold with age driver for an injury risk factor of 30 percent.

shown in Fig. 9) can produce an IRF, respectively, of 30 and 50 percent. Fig. 11 and Eq. (8) shows the relationship between the acceleration threshold $A_{30\ \mathrm{percent}}$ and the driver's age:

$$A_{30\ \mathrm{percent}} = -0.15\ \mathrm{year} + 11.48. \tag{8}$$

By considering an IRF level 30 percent, Fig. 11 shows that the amplitude of vibration must be reduced to $4.5\,\mathrm{m/s^2}$ when the driver is 45 years old and to $2.1\,\mathrm{m\,s^{-2}}$ when the driver is 65 years old (apparent density of $0.18\,\mathrm{g\,cm^{-3}}$), if the excitation is maintained at the natural frequency of the lumbar spine, as is the case under shock or random excitation. Therefore an acceleration amplitude of $2.1\,\mathrm{m\,s^{-2}}$ can be considered as a limit in order to avoid any injury risk and this whatever the age of driver.

6. Conclusion

In the research described in this paper the aims were to study the dynamic behaviour and stress distribution in the lumbar vertebrae when exposed to low-amplitude mechanical vibrations, and, in so doing, help for validating the assumption that whole-body vibration can induce microfractures in the bony elements of the spine, which, in turn, can lead to adverse health effects. A finite element numerical model of the lumbar spine has been developed using a parametric model. Two other models, representing the lumbar and thoracic

spine and L4–5 motion segments, were generated to predict the natural frequencies and to validate the parametric model. The dynamic model is aimed at computing the modal analysis, the response transmissibility and the dynamic mechanical stresses of the lumbar spine produced by whole-body vibration, in order to evaluate the potential risk of adverse health effects for professional drivers while in a seated position. Furthermore, the computed stress/strain distributions identify the osseous locations most susceptible for damaging. This parametric finite element model has been validated by using published results of natural frequencies and transmissibility. A new damage index has been developed for predicting the risk of exceeding a certain percentage of the material's ultimate stress capacity and consequently developing microfractures (noted IRF) under an excitation coming from the seat for any given vibratory amplitude. This study has revealed a quantitative relationship between the dynamic stresses and the acceleration amplitude measured at the seat and another between the IRF and acceleration and ageing. It is found that acceleration amplitudes greater than 4. $5\,m/s^2$ could produce a high probability of injury. In order to compare the computed forces with those published in literature, acceleration amplitudes of $3\,m\,s^{-2}$ have been applied to the seat in order to calculate the equivalent compressive force at the segment L3–L4. The estimated equivalent compressive force at segment L3–L4 is about 1030 N. The risk of adverse health is more significant if the apparent density is lower than $0.23\,g\,cm^{-3}$ (about $0.18\,g\,cm^{-3}$). These effects are related to the age of drivers and this study confirmed that old drivers present a more significant risk of fracture than the young's one. If an injury risk factor of about 30 percent is defined as the limit of endurance in order to avoid fatigue problems, the results show that drivers older than 45 years old are susceptible to long term injury. An excitation acceleration of $2\,m\,s^{-2}$ applied to the seat have been found as a threshold limit in order to avoid any risk of fracture, whatever the age of the driver. For the acceleration threshold of $2\,m\,s^{-2}$, the IRF was found ranging from 12 percent for a young driver to 30 percent for an old driver. The future of this research is aimed at investigating, by a statistical approach, the effect of the following parameters: driving posture, body weight, bone structure, apparent density (age), acceleration level and damping rate on dynamic stresses and on the health risk (IRF) due to WBV. The study will enable the evaluation of lumbar spine mechanical fatigue when exposed to the continuous whole-body vibration for the prediction of the vertebral lifespan when subject to long-term exposure to low-frequency and low-amplitude dynamic loads.

Acknowledgements

The authors gratefully acknowledge the financial support provided by the Institut de Recherche en Santé et Sécurité du Travail (IRSST-Montréal) and the Natural Sciences and Engineering research council of Canada (NSERC) through grants to graduate students.

References

[1] M. Bovenzi, C. Hulshof, An updated review of epidemiologic studies on the relationship between exposure to whole-body vibration and low back pain, *Journal of Sound and Vibration* 215 (4) (1998) 595–612.
[2] M.J. Griffin, *Handbook of Human Vibrations*, Academic Press, London, 1990.
[3] S. Lings, C. Leboeuf, Whole-body vibration and low back pain: a systematic, critical review of the epidemiological literature 1992–1999, *International Archives of Occupational and Environmental Health* 73 (2000) 290–297.
[4] M.H. Pope, D.G. Wilder, M. Magnusson, Possible mechanics of low back pain due to whole-body vibration, *Journal of Sound and Vibration* 215 (4) (1998) 687–697.
[5] M.L. Magnusson, M.H. Pope, Development of a protocol for epidemiological studies of whole-body vibration and musculoskeletal disorders of the lower back, *Journal of Sound and Vibration* 215 (4) (1998) 643–651.
[6] C. Hulshof, B. Van Zanten Veldhuijzen, Whole-body vibration and low-back pain, *International Archives of Occupational and Environmental Health* 59 (1987) 205–220.
[7] P.E. Boileau, Whole-body vibration exposure and its role in the aetiology of low back pain, *Travail et Santé* 18 (1) (2002) 31–35 (in French).
[8] J. Sandover, The fatigue approach to vibration and health: it is a practical and viable way of predicting the effects on people, *Journal of Sound and Vibration* 215 (4) (1998) 699–721.
[9] M. Thomas, A.A. Lakis, S. Sassi, Adverse health effects of long-term whole-body random vibration exposure, recent research, development in sound and vibration, *Transworld Research Network* 2 (2004) 55–73.
[10] M.H. Pope, T.H. Hansson, Vibration of the spine and low back pain, *Clinical Orthopedics and Related Research* 279 (1992) 49–59.

[11] T.M. Hansson, T. Keller, R. Johnson, Mechanical behaviour of human lumbar spine. Fatigue strength during dynamic compressive loading, *Journal of Orthopedic Research* 5 (4) (1987) 479–487.
[12] P. Brinckmann, M. Biggeman, D. Hilweg, Fatigue fracture of human lumbar vertebrae, *Clinical Biomechanics* 3 (Suppl. 1) (1988) 1–23.
[13] H. Seidel, R. Bluthner, B. Hinz, On the health risk of the lumbar spine due to whole-body vibration. The theoretical approach, experimental data and evaluation of whole-body vibration, Federal Institute for Occupational Safety and Health, *Journal of Sound and Vibration* 215 (4) (1998) 723–741.
[14] H. Ayari, M. Thomas, S. Doré, Statistical model development for predicting life time of lumbar rachis, according to cyclic stresses, age and bone density, *IRSST, Pistes* 7 (2) (2005) 1–14 (in French).
[15] T. Hansson, B. Roos, Microcalluses of the trabeculae in lumbar vertebrae and their relation to the bone mineral content, *Spine* 6 (1981) 375–380.
[16] D. Vashishth, J. Koontz, S.J. Qiu, D. Lundin-Cannon, Y.N. Yeni, M.B. Schaffler, D.P. Fyhrie, In vivo diffuse damage in human vertebral cancellous bone, *Bone* 26 (2000) 147–152.
[17] T. Wenzel, M. Schaffler, D. Fyhrie, In-vivo cancellous microcracks in human vertebral bone, *Bone* 19 (1996) 89–95.
[18] H. Dupuis, G. Zerlett, Acute effects of mechanical vibration, in: *The Effects of Whole-Body Vibration*, Springer, Berlin, Heidelberg, 1986, pp. 12–86 (ISBN: 0387165843).
[19] P.E Boileau, S. Rackheja, X. Yang, I. Stiharu, Comparison of biodynamic response characteristics of various human body models as applied to seated vehicle drivers, *Noise and Vibration Worldwide*, October 1997, pp. 8–15.
[20] H. Dupuis, Medical and occupational preconditions for vibration-induced spinal disorders: occupational disease no. 2110 in Germany, *International Archives of Occupational and Environmental Health* 66 (2) (1994) 303–308.
[21] International Organization for Standardization ISO 5982, Range of idealized values to characterise seated-body biodynamic response under vertical vibration, *Mechanical Vibration and Shock*, second ed., Geneva, Switzerland, 2001, 24pp.
[22] International Organization for Standardization ISO 7962, Mechanical transmissibility of the human body in the z direction, *Mechanical Vibration and Shock*, first ed., Geneva, Switzerland, 1987, 15pp.
[23] International Organization for Standardization ISO 2631-1, Evaluation of human exposure to whole-body vibration—part 1: general requirements, *Mechanical Vibration and Shock*, Geneva, Switzerland, 1997, 22pp.
[24] M. Kasra, A. Shirazi, G. Drouin, Dynamics of human lumbar intervertebral joints. Experimental and finite-element investigations, *Spine* 17 (1) (1992) 93–102.
[25] V.K. Goel, B.T. Monroe, L.G. Gilbertson, P. Brinckmann, Finite element analysis of the L3–L4 motion segment subjected to axial compressive loads, *Spine* 20 (6) (1995) 689–698.
[26] O. Izambert, D. Mitton, M. Thourot, F. Lavaste, Dynamic stiffness and damping of human intervertebral disc using axial oscillatory displacement under a free mass system, *European Spine Journal* 12 (6) (2003) 562–566.
[27] W.Z. Kong, V.K. Goel, Ability of the finite element models to predict response of human spine to sinusoidal vertical vibration, *Spine* 28 (17) (2003) 1961–1967.
[28] S. Kitazaki, M.J. Griffin, A modal analysis of whole-body vertical vibration, using a finite element model of the human body, *Journal of Sound and Vibration* 200 (1) (1997) 83–103.
[29] B. Buck, H. Woelfel, Dynamic three-dimensional finite element model of a sitting man with a detailed representation of the lumbar spine and muscles, in: J. Middleton (Ed.), *Computer Methods in Biomechanical and Biomedical Engineering*, Vol. 2, 1998, pp. 451–463.
[30] M. Fritz, Description of the relation between the forces acting in the lumbar spine and whole-body vibrations by means of transfer functions, *Clinical Biomechanics* 15 (2000) 234–240.
[31] S. Pankoke, J. Hofmann, H. Woelfel, Determination of vibration-related spinal loads by numerical simulation, *Clinical Biomechanics* 16 (1) (2001) S45–S56.
[32] M. Verver, J. Van Hoof, C. Oomens, N. Van De Wouw, J. Wismans, Estimation of spinal loading in vertical vibrations by numerical simulation, *Clinical Biomechanics* 18 (2003) 800–811.
[33] J. Sandover, Dynamic loading as a possible source of low-back disorders, *Spine* (8) (1983) 652–659.
[34] F. Lavaste, W. Skalli, S. Robin, Three-dimensional geometrical and mechanical modelling of the lumbar spine, *Journal of Biomechanics* 25 (10) (1992) 1153–1164.
[35] J. Berry, J. Moran, W. Berg, A morphometric study of human lumbar and selected thoracic vertebrae, *Spine* 12 (1987) 362–367.
[36] P. Dolan, M.A. Adams, Recent advances in lumbar spinal mechanics and their significance for modelling, *Clinical Biomechanics* 16 (1) (2001) 8–16.
[37] D.N. Joanes, Dynamic compressive properties of human lumbar intervertebral joints: a compression between fresh and thawed specimens, *Journal of Biomechanics* 21 (5) (1988) 425–433.
[38] T. Sonoda, Studies on the strength for compression, tension and torsion of human vertebral column, *Journal of Biomechanics, Kyoto Prefectural University of Medicine* 71 (1962) 659–702.
[39] J.B. Morrison, D.G. Robinson, J.J. Nicol, G. Roddan, S.H. Martin, M.J.N. Springer, B.J. Cameron, J.P. Albano, A biomechanical approach to evaluating the health effects of repeated mechanical shocks, *Research and Technology Organization the Human Factor and Medicine Panel* 1 (24) (1998) 1–8.
[40] L.-X. Guo, E.-C. Teo, Prediction of the modal characteristics of the human spine at resonant frequency using finite element models, *Journal of Engineering in Medicine, Proceedings of the IMech* 219 (H) (2005) 230–241.
[41] B. Hinz, R. Bluethner, G. Menzel, H. Seidel, Estimation of disc compression during transient whole-body vibration, *Clinical Biomechanics* 9 (4) (1993) 263–271.

[42] S. Ruth, F. Allan, P. Randal, Effect of loading rate on endplate and vertebral body strength in human vertebrae, *Journal of Biomechanics* 36 (2003) 1875–1881.
[43] R.W. McCalden, J.A. McGeough, C.M. Court-Brown, Age-related changes in the compressive strength of cancellous bone: the relative importance of changes in density and trabecular architecture, *Journal of Bone and Joint Surgery* 79A (3) (1997) 421–427.
[44] D.L. Kopperdahl, M. Tony, Yield strain behavior of trabecular bone, *Journal of Biomechanics* 31 (1998) 601–608.
[45] S.J. Ferguson, S. Thomas, Biomechanics of the aging spine, *European Spine Journal* 12 (Suppl. 2) (2003) S97–S103.
[46] M.P. Ettinger, Aging bone and osteoporosis ''strategies for preventing fractures in the elderly,'' *Archives of Internal Medicine* (2003) 163.
[47] E.R. Myers, S.E. Wilson, Biomechanics of osteoporosis and vertebral fracture, *Spine* 22 (1997) 25–31.
[48] R. Carter Dennis, E. Caler William, Uniaxial fatigue of human cortical bone the influence of tissue physical characteristics, *Journal of Biomechanics* 14 (1981) 461–470.
[49] R.R. Coermann, The mechanical impedance of the human body in sitting and standing position at low frequencies, *Human Factors* 1 (1962) 227–253.
[50] International Organization for Standardization ISO 2631-5, Evaluation of human exposure to whole-body vibration—part 5: Method for evaluation of vibration containing multiple shocks, *Mechanical Vibration and Shock*, Geneva, Switzerland, 2004, 21pp.